High proton conductivity of magnetically ordered 2D oxalate-bridged [$Mn^{II}Cr^{III}$] coordination polymers with irregular topology

Ana Lozančić,[a] *Sanja Renka,*[a] *Dario Barišić,*[b] *Sanja Burazer,*[a] *Krešimir Molčanov,*[a]

Damir Pajić[b] *and Marijana Jurić*[a,]*

[a]Ruđer Bošković Institute, Bijenička cesta 54, 10000 Zagreb, Croatia

[b]Department of Physics, Faculty of Science, University of Zagreb, Bijenička cesta 32,

10000 Zagreb, Croatia

ABSTRACT. Two heterometallic coordination polymers $\{[NH(CH_3)_2(C_2H_5)]_8[Mn_4Cl_4Cr_4(C_2O_4)_{12}]\}_n$ (**1**) and $\{[NH(CH_3)(C_2H_5)_2]_8[Mn_4Cl_4Cr_4(C_2O_4)_{12}]\}_n$ (**2**) were obtained by slow evaporation of an aqueous solution containing the building block $[A]_3[Cr(C_2O_4)_3]$ [A = $(CH_3)_2(C_2H_5)NH^+$ or $(CH_3)(C_2H_5)_2NH^+$] and $MnCl_2{\cdot}2H_2O$. The isostructural compounds comprise an irregular two-dimensional (2D) oxalate-bridged anionic layers $[Mn_4Cl_4Cr_4(C_2O_4)_{12}]_n^{\delta n-}$ with a Shubnikov plane net **fes** topology designated as $(4{\cdot}8^2)$, interleaved by the hydrogen-bonded templating cations $(CH_3)_2(C_2H_5)NH^+$ (**1**) or $(CH_3)(C_2H_5)_2NH^+$ (**2**). They exhibit remarkable humidity-sensing properties and very high proton conductivity at room temperature [1.60×10^{-3} $(\Omega{\cdot}cm)^{-1}$ at 90% RH of **1** and 9.6×10^{-4} $(\Omega{\cdot}cm)^{-1}$ at 94% RH of **2**]. The layered structure facilitates the uptake of water molecules, which contributes to the enhancement of proton conductivity at high RH. The better proton transport observed in **1** compared to **2** can be tentatively attributed to the higher hydrophilicity of the cations $(CH_3)_2(C_2H_5)NH^+$, which is closely related to the affinity for water molecules. The original topology of the anionic networks in both compounds leads to the development of interesting magnetic phases upon cooling. The magnetically ordered ground state can be described as coupling of ferromagnetic spin chains in which Mn^{2+} and Cr^{3+} ions are bridged by bis(bidentate) oxalate groups into antiferromagnetic planes through monodentate-bidentate oxalate bridges in the layers, which are triggered to long-range order below temperature 4.45 K *via* weaker interlayer interactions.

INTRODUCTION

The chemistry of an enormous number of coordination polymers of different structures, dimensionality and nuclearity is the basis for the development of molecular-based materials that combine two (or more) physical properties of interest, especially for the improvement and extension of molecular magnetism toward multifunctional systems.[1−6]

Recently, porous crystalline metal–organic frameworks (MOFs) and porous coordination polymers (PCPs) have attracted much attention as a new class of solid-state proton conductors due to their crystallinity, designability, and high porosity, finding broad applications in electrochemical devices, as a key component for the safety and efficiency of fuel cells.[7−13] In addition, proton-conducting MOFs with switching behavior have gained increasing attention in recent years due to their potential applications in smart devices, resistive switches, and field-effect transistors.[14] In most cases, proton-conductive coordination polymers can be classified into different types depending on the proton source and hopping site. The simplest method to introduce proton carriers is to incorporate a counterion such as hydronium (H_3O^+), ammonium [NH_4^+, $(CH_3)_2NH_2^+$,...] or an anion (SO_4^{2-}) during synthesis, resulting in the charged compounds. The counterions form the hydrogen-bonding arrays with the guest water or other constituents of compound, creating proton-conducting pathways. Conductivity can also be achieved by introducing functionalized structural components such as noncoordinated functional groups in organic ligands (e.g., -OH, -NH_2, -COOH, -SO_3H, and -PO_3H_2) or by coordinating a metal center with functional molecules such as H_2O, EtOH, and imidazole, which is achieved by using predesigned components or postsynthetic modification. Furthermore, due to porosity functional guest molecules such as acid molecules or protic organic molecules can be incorporated in the metal-organic frameworks.[7,8,9,11,12] The excellent proton conductivity of some metal-organic

compounds is closely related to humidity as a conductive medium, since interesting networks of hydrogen bonds are formed with guest molecules. Usually, this medium is H_2O molecules, which form a degenerate conjugated acid-base system and have an efficient hydrogen-bonding ability through two proton donor and two acceptor sites with tetrahedral geometry. Therefore, common water-mediated proton conductors require high humidity at mild temperature conditions.[15–20]

A very important role in the design and synthesis of multifunctional materials is played by the oxalate moiety, $C_2O_4^{2-}$, due to its various possibilities of coordination to metal centers and its ability to mediate electronic effects between paramagnetic metal ions. The synthetic strategy for preparation of (hetero)polynuclear species is "building block chemistry", in which a molecular anionic ligand, very often the tris(oxalato)metalate anion, $[M^{III}(C_2O_4)_3]^{3-}$, is used as a ligand towards other metal cations, in particular, to obtain two-dimensional (2D) and three-dimensional (3D) extended systems of the general formula $[M_a^{II/III}M_b^{I/II}(C_2O_4)]_n^{2n-/n-}$, showing different magnetic ordering. The topology of these compounds is controlled by templating counterions, and by combining the intrinsic properties of the host, especially the magnetic ones, with additional functionalities derived from the selected guest molecules, very interesting multifunctional properties can be obtained.[5,6,21–26] Using $[Cr(C_2O_4)_3]^{3-}$ as a building block, a series of mixed-metal assemblies $\{[NR_4][M^{II}Cr^{III}(C_2O_4)_3]\}_n$ (R = *n*-butyl; M^{II} = Mn, Fe, Co, Ni, Cu, Zn) was obtained, for which the ferromagnetic phase transition was observed up to 14 K;[23] the crystal structures of these assemblies were not known. Shortly afterwards, determination of the crystal structure of $\{[PR_4][Mn^{II}Cr^{III}(C_2O_4)_3]\}_n$ (R = phenyl) revealed a 2D structure, and the ferromagnetic behaviour was confirmed.[24]

Since the oxalate-based compounds with regular structures and stable frameworks usually exhibit good water and chemical durability under the influence of humidity and temperature,

they have been extensively studied as proton conductive materials. In addition, the oxygen atoms of the oxalate group can form complex hydrogen-bonded networks, which are more than suitable for proton conduction.[15–20]

In our previous works, we reported structural and, in particular, magnetic properties of heterometallic oxalate-bridged coordination polymers of different dimensionality obtained using $[M^{III}(C_2O_4)_3]^{3-}$ (M^{III} = Cr, Mn, and Fe) as building blocks.[25–31] Motivated by these results and those of the one-dimensional (1D) oxalate-bridged coordination polymer $\{[NH(CH_3)_2(C_2H_5)][FeCl_2(C_2O_4)]\}_n$, which exhibits very high proton conductivity at room temperature and exceptional humidity-sensing properties,[32] we have now focused on the preparation of novel heterometallic oxalate-bridged compounds that would exhibit magnetic order and proton conductivity as a new functionality by incorporating proton carriers as counterions into the oxalate networks. This was achieved by using an aqueous solution of $[A]_3[Cr(C_2O_4)_3]$ [A = $(CH_3)_2(C_2H_5)NH^+$ or $(CH_3)(C_2H_5)_2NH^+$] as a complex ligand in reaction with Mn^{2+} ions, thereby simultaneously involving proton carriers in the synthesis of coordination polymers, resulting in the charged 2D frameworks $\{[A]_8[Mn_4Cl_4Cr_4(C_2O_4)_{12}]\}_n$ [A = $(CH_3)_2(C_2H_5)NH^+$ (**1**); A = $(CH_3)(C_2H_5)_2NH^+$ (**2**)]. In this work, we report structural features of the prepared compounds **1** and **2**, which are reflected in the magnetic and electrical properties of the new oxalate-based $[Mn^{II}Cr^{III}]$ coordination polymers.

EXPERIMENTAL SECTION

Materials and Physical Measurements. All used chemicals were procured from commercial sources and used without further purification. The salt $K_3[Cr(C_2O_4)_3]\cdot 3H_2O$ was prepared by the method described in the literature.[33] The precursor salt $Ag_3[Cr(C_2O_4)3]\cdot nH_2O$ was obtained from the corresponding potassium salt by metathesis.

The infrared spectra were recorded using KBr pellets by a Bruker Alpha-T spectrometer in the 4000–350 cm^{-1} range. Room temperature (RT) powder X-ray diffraction data (PXRD) were collected on a Malvern Panalytical Empyrean diffractometer in the scan range from 5° to 50° 2Θ, in reflection geometry. Prior to measurements, samples were ground with a pestle in an agate mortar to obtain fine powders. Program HighScoreXpert Plus (Version 4.5, March 2016) was used to compare the experimental and theoretical data. Thermal properties were investigated from RT to 900 °C in synthetic air, with a Shimadzu DTG-60H analyzer (heating rate of 5 $°C \cdot min^{-1}$).

Synthesis of the Precursors $[A]_3[Cr(C_2O_4)_3]$ [A = $(CH_3)_2(C_2H_5)NH^+$ or $(CH_3)(C_2H_5)_2NH^+$]. The *N,N*-dimethylethylamine (0.0328 mL; 0.3 mmol) or *N,N*-diethylmethylamine (0.0366 mL; 0.3 mmol) was mixed with 37% HCl (0.3 mmol; 1.5 mL) and reaction mixture was added dropwise to the aqueous solution (3.5 mL) of $Ag_3[Cr(C_2O_4)_3] \cdot nH_2O$ (0.0694 g; 0.1 mmol). The reaction mixtures were filtered due to the appearance of a white precipitate (AgCl). The remaining dark violet filtrates were used as a precursor for further reaction.

Synthesis of $\{[A]_8[Mn_4Cl_4Cr_4(C_2O_4)_{12}]\}_n$ [A = $(CH_3)_2(C_2H_5)NH^+$ (1); A = $(CH_3)(C_2H_5)_2NH^+$ (2)]. Compounds **1** and **2** were synthesized by the same basic procedure: to the prepared aqueous solution of the precursor $[NH(CH_3)_2(C_2H_5)]_3[Cr(C_2O_4)_3]$ or $[NH(CH_3)(C_2H_5)_2]_3[Cr(C_2O_4)_3]$ (0.100 mmol; 5 mL) was slowly added, with constant stirring, an aqueous solution of $MnCl_2 \cdot 2H_2O$ (0.019 g; 0.100 mmol; 5 mL). The glass with the clear solution is covered with parafilm, a few holes are made and left to evaporate at room conditions. After one week, the solution evaporates to dryness, and violete crystals of compound **1** or **2** appear at the bottom of the beaker. The crystals are mechanically separated, washed with absolute alcohol and air-dried [yield 43% (**1**) and 35% (**2**)]. IR data for **1** (KBr, cm^{-1}): 3431 (m), 3043 (m), 2996

(m), 2764 (m), 2484 (w), 1707 (s), 1681 (vs), 1633 (vs), 1458 (m), 1421 (s), 1341 (m), 1294 (m), 1188 (w), 1064 (w), 1023 (w), 995 (w), 924 (w), 907 (w), 816 (m), 808 (m), 778 (sh), 600 (sh), 543 (m), 480 (m), 419 (m). IR data for **2** (KBr, cm^{-1}): 3426 (m), 3035 (m), 3000 (m), 2769 (m), 2487 (w), 1707 (s), 1679 (vs), 1633 (vs), 1456 (m), 1419 (s), 1341 (m), 1293 (m), 1206 (w), 1172 (w), 1160 (w), 1060 (m), 1023 (w), 974 (w), 906 (m), 815 (m), 802 (m), 778 (sh), 595 (sh), 543 (s), 479 (m), 418 (s).

Single-Crystal X-ray Structural Study. The X-ray data for single crystals of compounds **1** and **2** were recorded by ω-scans on on a Rigaku Oxford Diffraction Synergy S diffractometer using CuK_α radiation at 297(2) K (**1**), and 296 K (**2**). Data reduction, including the multi-scan absorption correction, was performed by using the CrysAlisPRO[34] software package. The structures were solved using SHELXT[35] and refined with SHELXL-2017/1 within the WinGX software package.[36] The full-matrix least squares refinement was used to refine the models; all non-hydrogen atoms were refined anisotropically. Due to the large thermal motion of the dimethylethylammonium and diethylmethylammonium cations, their C–C and C–N bonds were restrained to 1.54(4) and 1.47(4) Å, respectively. Hydrogen atoms were constrained to a 'riding model'.

Molecular geometry calculations were carried out using PLATON[37] and the figures were made by the use of the CCDC-Mercury.[38] Analyses of topology were done using the program package TOPOS PRO.[39] Crystallographic and refinement data for the structures reported in this paper are shown in Table 1.

Electrical Study. The conductivity of compounds **1** and **2** was measured by impedance spectroscopy (Novocontrol Alpha-AN Dielectric Spectrometer, Novocontrol Technologies GmbH & Co. KG, Hundsangen, Germany) in a frequency range from 0.01 Hz to 1 MHz at

different temperature and humidity conditions: 46% (air, ambient conditions), 75%, 84% and 93%. The relative humidity (RH) inside the sample cell was obtained using saturated aqueous solutions of different salts: NaCl (RH = 75%), KCl (RH = 84%), and KNO_3 (RH = 93%). In addition, the impedance spectra of compounds **1** and **2** were measured in dry nitrogen at temperatures from −50 °C to 30 °C (temperature step: 10 °C) and in the frequency range from 0.01 Hz to 1 MHz. The measurements were performed on polycrystalline sample pressed into pellet of approximate thickness 0.8 mm. For the electrical contacts, gold electrodes (3.8 mm in diameter) were sputtered on the opposite surfaces of the pellet. The impedance spectra were analysed by equivalent circuit modelling using the complex nonlinear least-squares fitting procedure (ZView software). From the values of electrical resistance (R) and electrode dimensions (A is the electrode area, and d is the sample thickness) the DC conductivity was calculated according to the following equation: $\sigma_{DC} = d/(A \cdot R)$. The experimental PXRD pattern of a polycrystalline samples **1** and **2** are consistent with those calculated from the single-crystal X-ray diffraction data (Figures S1 and S2), confirming the purity and the homogeneity of the bulk samples.

Table 1 Crystallographic Data, Structure Refinement Details and Data Collection for Compounds $\{[NH(CH_3)_2(C_2H_5)]_8[Mn_4Cl_4Cr_4(C_2O_4)_{12}]\}_n$ (**1**) and $\{[NH(CH_3)(C_2H_5)_2]_8[Mn_4Cl_4Cr_4(C_2O_4)_{12}]\}_n$ (**2**).

Compound	**1**	**2**
Empirical formula	$C_{56}H_{96}Cl_4Cr_4Mn_4N_8O_{48}$	$C_{64}H_{112}Cl_4Cr_4Mn_4N_8O_{48}$
*f*w (g mol^{-1})	2218.97	2331.18
Colour	violet	violet
Crystal dimensions (mm)	0.30 × 0.15 × 0.09	0.18 × 0.17 × 0.14
Space group	$P2_1$	$P2_1$
a (Å)	13.8321(4)	14.1863(3)
b (Å)	17.1042(4)	17.3479(3)
c (Å)	20.4209(4)	20.4140(4)
α (°)	90	90
β (°)	91.874(2)	91.937(2)
γ (°)	90	90
Z	2	2
V (Å$^{3)}$	4828.7(2)	5021.07(17)
D_{calc} (g cm^{-3})	1.526	1.542
λ (Å)	1.54184 (Cu*K*α)	1.54184 (Cu*K*α)
μ (mm^{-1})	9.511	9.176
F(000)	2272	2400
Θ range (°)	3.803–80.226	3.344–80.546
T (K)	297(2)	296(2)
Diffractometer type	Synergy S	Synergy S
Range of *h*, *k*, *l*	$-17 < h < 16$ $-15 < k < 21$ $-22 < l < 26$	$-16 < h < 18$ $-21 < k < 22$ $-25 < l < 25$
Reflections collected	42337	83243
Independent reflections	15078	19946
Observed reflections ($I \geq 2\sigma$)	10704	15278
R_{int}	0.0611	0.0696
R, w*R* [I ≥ 2σ(I)]	0.0795, 0.1607	0.0761, 0.1978
R, w*R* [all data]	0.0543, 0.1431	0.0971, 0.2188
Goodness-of-fit	1.028	1.038
Absorption correction	multi-scan	multi-scan
No. of parameters, restraints	1117, 47	1189, 41
H atom treatment	constrained	constrained
$\Delta\rho_{max}$, $\Delta\rho_{min}$ (e Å^{-3})	0.377; –0.435	2.058, –0.962

Magnetic Study. The magnetization of polycrystalline powder samples (Figures S1 and S2) of compounds **1** and **2** was measured using a MPMS3 commercial superconducting quantum interference device (SQUID) magnetometer. The temperature dependence of magnetization *M*(*T*) was measured from 1.8 to 300 K in different applied magnetic fields, using two modes for each field: measurements after the zero field cooling (ZFC) and field cooling (FC). The field

dependence of the magnetization $M(H)$ was measured at different stable temperatures with a magnetic field up to 70 kOe in order to obtain the isothermal magnetic hysteresis loops. The powders were placed in gelatine ampoules whose moment was also measured, and the magnetic moments of the samples were taken from the measurements after corrections for the ampoule moment and the contribution of the core electrons. AC magnetic susceptibility χ_{ac} was measured with an excitation field of frequency 1 Hz and amplitude 5 Oe, also with the MPMS3.

RESULTS AND DISCUSSION

Molecular and Crystal Structures of Compounds 1 and 2. The violete polyhedral crystals of compounds $\{[A]_8[Mn_4Cl_4Cr_4(C_2O_4)_{12}]\}_n$ [A = $(CH_3)_2(C_2H_5)NH^+$ (**1**) and A = $(CH_3)(C_2H_5)_2NH^+$ (**2**)] were obtained by slow evaporaion of an aqueous solution containing building block $[A]_3[Cr(C_2O_4)_3]$ [A = $(CH_3)_2(C_2H_5)NH^+$ or $(CH_3)(C_2H_5)_2NH^+$] and $MnCl_2{\cdot}2H_2O$, in the molar ratio 1 : 1. In order to simultaneously include alkyl-ammonium counterions as proton carriers and overcome problems during the synthesis, we have employed a procedure in which an aqueous solution of $[Cr(C_2O_4)_3]^{3-}$ is used as a precursor containing $(CH_3)_2(C_2H_5)NH^+$ or $(CH_3)(C_2H_5)_2NH^+$ as counterions instead of the more common NH_4^+ or K^+.[25−29] The obtained crystals are moderetaly air-stable and very soluble in water, and not in commom organic solvents.

The isostructural compounds $\{[NH(CH_3)_2(C_2H_5)]_8[Mn_4Cl_4Cr_4(C_2O_4)_{12}]\}_n$ (**1**) and $\{[NH(CH_3)(C_2H_5)_2]_8[Mn_4Cl_4Cr_4(C_2O_4)_{12}]\}_n$ (**2**), which crystallize in the polar space group $P2_1$ (Table 1), comprise an irregular 2D oxalate-bridged anionic layers $[Mn_4Cl_4Cr_4(C_2O_4)_{12}]_n^{\delta n-}$ parallel to (010), with a Shubnikov plane net **fes** topology designated as $(4{\cdot}8^2)$ (Figures 1a and 1b),[39] interleaved by the hydrogen-bonded templating cations $(CH_3)_2(C_2H_5)NH^+$ (**1**) or $(CH_3)(C_2H_5)_2NH^+$ (**2**) (Figures 1c and 1d).

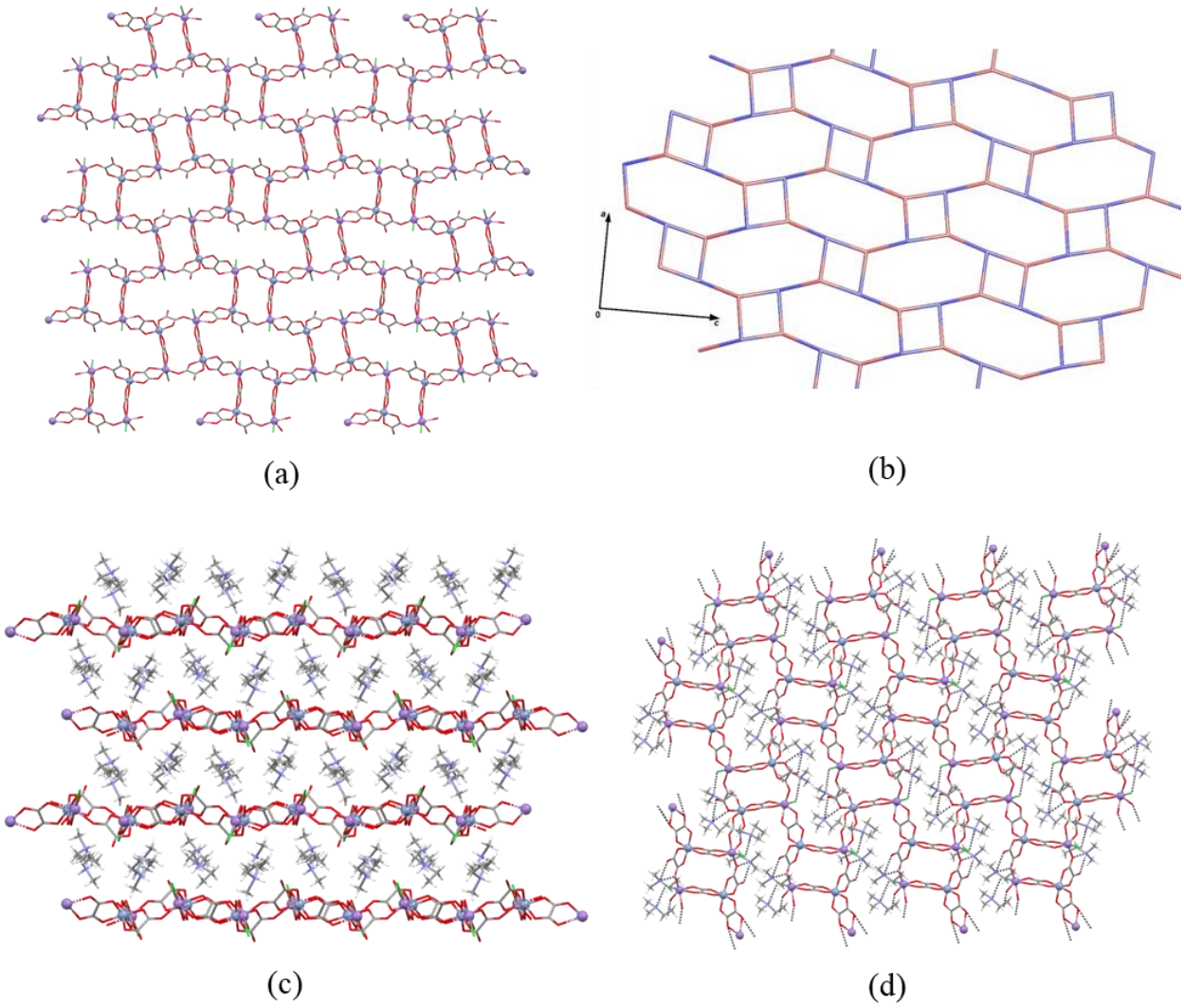

Figure 1. (a) 2D anionic network $[Mn_4Cl_4Cr_4(C_2O_4)_{12}]_n^{8n-}$ of compound **1** in the (010) plane; (b) Underlying graph with a Shubnikov plane net **fes** topology designated as $(4{\cdot}8^2)$ in coordination polymers **1** and **2**. Nodes corresponding to the Mn and Cr atoms are shown in red and blue, respectively; (c) Heterometallic layers interleaved by the templating cations $(CH_3)_2(C_2H_5)NH^+$; (d) Hydrogen-bonded $(CH_3)_2(C_2H_5)NH^+$ cations to the oxalate-bridged layer in the *c*-axis.

These compounds exhibit a 2D coordination network that is different from the known 2D (6,3) and 3D (10,3) oxalate-bridged extended systems of the general formula $[M^{II/III}{}_aM^{I/II}{}_b(C_2O_4)_3]_n^{2n-/n}$, which were obtained using tris(oxalato)metalate $[M^{III}(C_2O_4)_3]^{3-}$ anion

(M^{III} = V, Cr, Mn, Fe, Ru or Rh) as a ligand towards other metal cations.[21–26,30,31] These known layered 2D honeycomb structures were obtained with bulky organic cations $[XR_4]^+$ (X = N and P; R = aryl and alkyl) or even the decamethylmetallocenium unit $[A(Cp^*)_2]^+$ (A = Fe and Co; Cp* = pentamethylcyclopentadienyl).[21–25] Interestingly, using ammonium as template cations of $[Cr(C_2O_4)_3]^{3-}$ building block, two 3D coordination compounds with unusual Mn^{II}/Cr^{III} ratio, and original topology of the anionic network were prepared.[40,41]

Crystal structure analysis shows that the asymmetric unit of **1** or **2** consists of four independent $[Cr(C_2O_4)_3]^{3-}$ building blocks coordinated to the four independent manganese(II) ions and eight cations $(CH_3)_2(C_2H_5)NH^+$ and $(CH_3)(C_2H_5)_2NH^+$, respectively (Figures 2, S3 and S4). Each chromium(III) atom in both compounds is coordinated by six O atoms of three bridging oxalate ligands that have an approximately octahedral coordination geometry; the Cr–O distances are in the range of the lengths in similar compounds containing the same tris(oxalate) moiety.[27–29] Selected bond distances are summarized in Table S2. In this way, each chromium(III) ion is linked to three manganese(II) ions, but two different bridging modes of the oxalate groups are observed: two oxalate groups of the $[Cr(C_2O_4)_3]^{3-}$ unit are bidentatly and one is monodentatly coordinated to the manganese(II) atoms. This results in a layer in a plane (010) consisting of alternating, almost regular tetragonal $[Cr_2Mn_2]$ and octagonal rings $[Cr_4Mn_4]$ (Figures 1a, 1b and 1d).

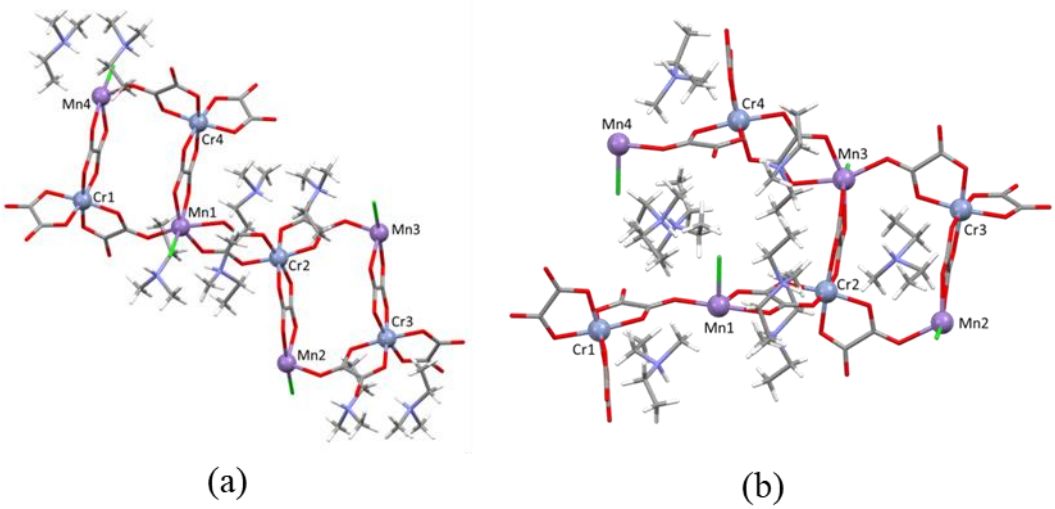

Figure 2. Asymmetric unit $[A]_8[Mn_4Cl_4Cr(C_2O_4)_{12}]$ of (a) compound **1** [A = $(CH_3)_2(C_2H_5)NH^+$] and (b) compound **2** [A = $(CH_3)(C_2H_5)_2NH^+$].

The manganese(II) ions display octahedral coordination involving two O atoms from bis(bidentate) oxalate bridge [Mn–O distances ranging from 2.174(6) to 2.334(6) Å for compound **1** (on average 2.241 Å) and from 2.203(7) to 2.307(7) Å for compound **2** (on average 2.248 Å); Table S1], one O atom of the oxalate group that act as monodentate-bidentate ligand [Mn–O distances ranging from 2.130(6) to 2.175(5) Å for compound **1** (on average 2.158 Å) and from 2.164(7) to 2.176(7) Å for compound **2** (on average 2.167 Å); Table S1], and one O atom from other bis(bidentate) oxalate group [Mn–O distances ranging from 2.175(6) to 2.215(6) Å for compound **1** (on average 2.198 Å) and from 2.195(7) to 2.225(7) Å for compound **2** (on average 2.209 Å); Table S1] from three different $[Cr(C_2O_4)_3]^{3-}$ units, together with another O atom from same bis(bidentate) bridge [Mn–O distances ranging from 2.237(6) to 2.255(7) Å for compound **1** and from 2.239(7) to 2.264(7) Å; Table S1] and chloride atoms [Mn–Cl distances ranging from 2.402(3) to 2.428(3) for compound **1** and from 2.416(3) to 2.429(3) Å for compound **2**; Table S1] in the apical position. The shortest Mn–O distance corresponds to the

monodentate coordination modes.[40] Thus, each manganese(II) ion is connected to the three $[Cr(C_2O_4)_3]^{3-}$ units.

Cations $(CH_3)_2(C_2H_5)NH^+$ or $(CH_3)(C_2H_5)_2NH^+$ interact with bimetallic layer through hydrogen bonding to oxygen atoms of the monodentate-bidentate oxalate groups and chloride atoms coordinated to manganese(II) atom; four asymmetric cations are linked by N–H···Cl, and other four by two N–H···O_{ox} bonds (Table S2).

The distances between chromium(III) and manganese(II) ions through bis(bidentate) oxalate ligand are in the range 5.4282(19)–5.5165(16) Å for **1** and 5.450(2)–5.5257(19) Å for **2**, and those between chromium(III) and manganese(II) ions connected over bidentate-monodentate oxalate bridge are in the range 5.2319(16)–5.3883(17) Å for **1** and 5.2444(19)–5.406(2) Å for **2**.

The distances between two heterometallic anionic layers are 8.55 Å and 8.67 Å in **1** and **2**, respectively. These values are consistent with the interlayer separations of similar 2D $\{A[M_aM_b(C_2O_4)_3]\}_n$ compounds, which range from 9.96 to 6.34 Å, depending on the bulkiness of the cation.[42–45] The larger interlayer separation was observed in the compounds containing organometallic cations.[46–48] The shortest interlayer distance of 6.34 Å was found in compound $\{(H_2dab)[Zn_2(C_2O_4)_3]\cdot 2H_2O\}_n$ (dab = 1,4-diaminobutane), in which the H_2dab ions are incorporated in the cavities of the honeycomb framework as counterions,[43] and two water molecules are present in the interlayer space, indicating that compounds **1** and **2** have sufficient interlayer space for the inclusion of several water molecules. The shortest interlayer distance (7.90 Å) among the $[Mn^{II}Cr^{III}]$ complexes of this type has one with tri(3-hydroxypropyl)ammonium cations, $[NH(prol)_3^+]$, having folded, tripodal configuration.[45]

The TGA curves of **1** and **2** show almost single-step decomposition starting at ~200 °C and ending at ~600 °C (Figure S5). This step, followed by strong exothermic DTA maximum, could

be associated with the removal of alkyl-substituted ammonium and chloride ions together with the elimination of the oxalate groups. Crystalline products obtained by pyrolysis in the range 700–900 °C were explored by PXRD at RT and they correspond to the formation of the pure phase with cubic spinel structure $[Mn^{2+}][Mn^{3+}_{0.5}Cr^{3+}_{1.5}]O_4$ (167403-ICSD)[49] (Figure S6).

Infrared Study. The IR spectra of the prepared complexes are in agreement with the results of X-ray analysis: the presence of oxalate groups and alkyl-substituted ammonium cations can be inferred from the spectra (Figure S7). The absorption bands corresponding to the stretching vibrations of the uncoordinated (monodentate-bidentate mode) and coordinated [bis(bidentate) mode] CO groups of the oxalate ligands are summarized for both compounds in Table S3.[27–29,50] Due to the presence of alkyl-substituted cations in **1** and **2**, in addition to the bands around 1458 cm^{-1} in both compounds ascribed to the δ_s(C–H), the bands of medium intensity located at 3215–2850 cm^{-1} and 2840–2650 cm^{-1} could be recognized as ν(N–H) and $\nu_s(CH_2)$. The bands of medium intensity found in the region 1100–950 cm^{-1} in **1** and **2** originate from the C–N stretching.[51,52]

Proton Conductivity. Nyquist plots for samples **1** and **2** measured in a dry nitrogen atmosphere (~ 10% RH) are shown in Figure S8. The spectra consist of a well-defined semicircle corresponding to the conduction process through the bulk and a small spur at low frequencies, possibly related to the blocking of protons on the surface of the metallic electrodes. To obtain DC conductivity values, each spectrum was modelled by a corresponding equivalent electrical circuit consisting of a parallel combination of a resistor and a constant phase element (CPE 1), representing bulk response, and an additional constant phase element (CPE 2), representing the spur. From the model parameter of resistance (R) and electrode geometry, the DC conductivity

was calculated and found to be 7.75×10^{-9} $(\Omega \cdot cm)^{-1}$ and 3.90×10^{-7} $(\Omega \cdot cm)^{-1}$ at 30 °C and dry nitrogen atmosphere for **1** and **2**, respectively.

Samples of compounds **1** and **2** (Figures S1 and S2) were shown to be extremely sensitive to the humidity conditions exhibiting increase in σ_{DC} almost six and four orders of magnitude with increasing relative humidity, respectively (Figure 3). These features confirm that proton transport is responsible for the high conductivity of both compounds. The values of electrical conductivity of **1** at 75%, 84% and 90% of RH were found to be 1.69×10^{-7} $(\Omega \cdot cm)^{-1}$, 6.20×10^{-4} $(\Omega \cdot cm)^{-1}$ and 1.60×10^{-3} $(\Omega \cdot cm)^{-1}$, respectively, while those of **2** at 74%, 82% and 94% of RH 3.3×10^{-5} $(\Omega \cdot cm)^{-1}$, 3.56×10^{-5} $(\Omega \cdot cm)^{-1}$ and 9.6×10^{-4} $(\Omega \cdot cm)^{-1}$, respectively.

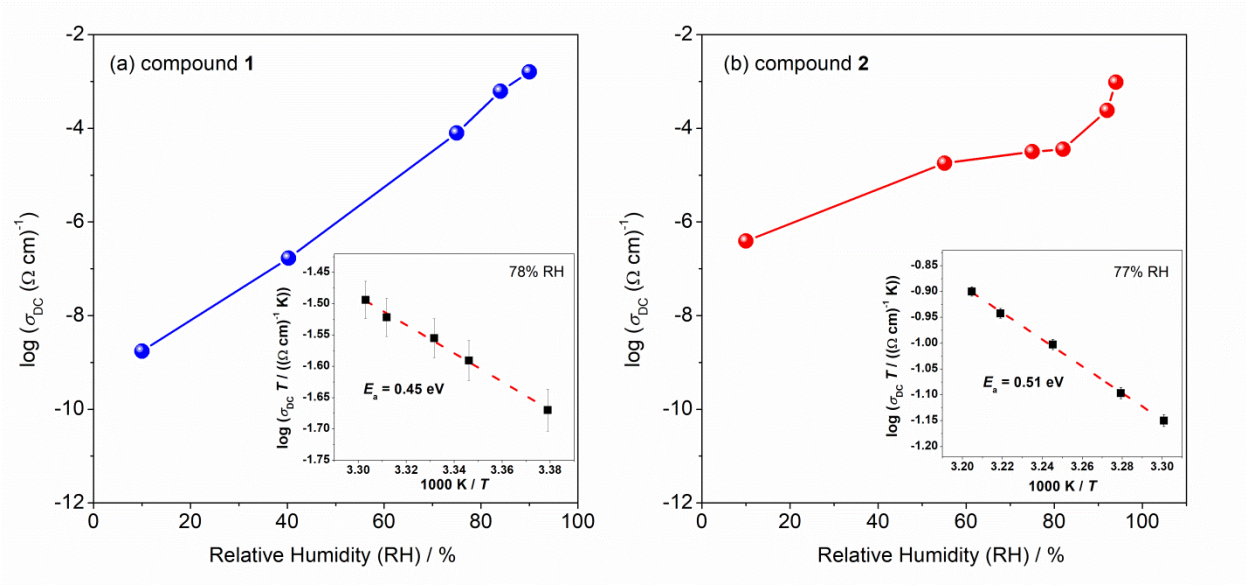

Figure 3. The proton conductivity as a function of relative humidity (RH) at room temperature of compound (a) $\{[NH(CH_3)_2(C_2H_5)]_8[Mn_4Cl_4Cr_4(C_2O_4)_{12}]\}_n$ (**1**) and (b) $\{[NH(CH_3)(C_2H_5)_2]_8[Mn_4Cl_4Cr_4(C_2O_4)_{12}]\}_n$ (**2**). The inset in (a) and (b) shows an Arrhenius-type plot of the DC conductivity with the corresponding value of activation energy for proton conductivity of **1** and **2** at 78% and 77% RH, respectively.

Insets in Figure 3a and b show Arrhenius temperature dependence of DC conductivity for compound **1** and **2** measured at 78 and 77 %RH, respectively. From the slope of the straight line, in the plot of $\log(\sigma_{DC}T)$ versus $1000/T$, activation energy for conduction process was calculated and found to be 0.45 eV for compound **1** and 0.51 eV for compound **2**. The obtained values are slightly higher than those typically attributed to a predominant Grotthuss mechanism ($E_a < 0.4$ eV), in which a proton moves within a hydrogen-bonded network.[19,20] So, the mechanism of proton conductivity of **1** and **2** is expected to be similar to that of proton hopping, suggesting, however, that conductivity is also due in part to another process, such as the direct diffusion of additional protons with water molecules in a vehicle mechanism.[53,54]

As shown in Figure S9, after the initial increase in conductivity, which occurs within the first four hours at 75% and 84% RH, the proton conductivity of both samples remains relatively stable over a period of 18 hours. However, at a higher humidity rate of 90%, the samples become deliquescent after 4 hours of measurement for **1** and 8 hours of measurement for **2**. These compounds have instability limits at similar humidity values and begin to deliquescent above the maximum allowable humidity.

Figures S10 and S11 show the experimental powder XRD patterns of **1** and **2** after being exposed to humidity, respectively. It can be seen that no changes were observed in the structures after treatment with humidity, indicating the stability of compounds **1** and **2**. In order to explore compounds as promising candidates for the development of solid-state electrolytes, their structural completeness must be ensured to maintain their natural functionalities and properties under operating conditions. Therefore, water stability is always a prerequisite for studying the proton conductivity of coordination polymers under humid conditions.[20]

The σ_{DC} values of 1.60×10^{-3} $(\Omega \cdot cm)^{-1}$ at 90% RH of **1** and 9.6×10^{-4} $(\Omega \cdot cm)^{-1}$ at 94% RH of **2** at 295 K are very high, especially first value, which is mostly higher than those reported for other studied 2D oxalate-based metal-organic frameworks in which a hydrogen-mediated bonding pathway is present (Table S4).[42,44,45,53–56] Moreover, only compound $\{(NH_4)_2(H_2adp)[Zn_2(C_2O_4)_3]\cdot 3H_2O\}_n$ exhibits a slightly higher conductivity [8×10^{-3} $(\Omega \cdot cm)^{-1}$; 98% RH] among the layered structures.[53] In the 3D oxalate-based networks the channels are mostly filled with ions and water, and these compounds generally show better proton conductivity (Table S4)[40,41,57-59] as $\{(NH_4)_4[MnCr_2(C_2O_4)_6]\cdot 4H_2O\}_n$[40] ($1.1 \times 10^{-3}$ $(\Omega \cdot cm)^{-1}$; 96% RH; 22 °C) and $\{[(CH_3)_2NH_2)_3(SO_4)]_2[Zn_2(C_2O_4)_3]\}_n$[58] ($4.2 \times 10^{-2}$ $(\Omega \cdot cm)^{-1}$; 98% RH; 25 °C).

As mentioned earlier, the periodic distances between the layers of **1** and **2** were determined to be 8.55 and 8.67 Å, respectively. According to the previous data of similar coordination polymers with periodic spacing that could adsorb water molecules in their interlayer, structures of compounds **1** and **2** should have enough space to accommodate several water molecules in their interlayers.[42,43] The hydrogen bonds formed by the bimetallic layer and the alkyl-substituted ammonium cations are only moderately effective for proton conduction, but the layered structure facilitates the uptake of water molecules, which contributes to the improvement of proton conduction at high RH of the studied compounds.

At high humidity rate, above ~70% RH, compound **1** exhibits better proton conductivity (more than 1.5 times) in comparison to the compound **2**. Based on the very similar crystal structures, this finding can be related to the higher hydrophilicity of the dimethylethyl ammonium cations in **1** compared to the diethylmetyl ammonium cations in **2**. In general, the hydrophilicity of the cationic R_3NH^+ ions decreases with increasing bulkiness of the residue and it affects the

interlayer hydrophilicity, which is closely connected with the affinity to water molecules and hence with the proton conduction in the coordination polymers.[42,57]

The results of thermogravimetric analysis of samples **1** and **2**, after exposure to a humid condition (80% RH) for several hours, demonstrate the amount of adsorbed water molecules (Figure S12); below 130 °C they showed a weight loss of 4.16% and 3.00%, due to the loss of 5 and 4 water molecules per formula, respectively, included in the interlayer space. The obtained values are in agreement with the results of the measured conductivity; compound **1** shows a better conductivity (1.67%) than compound **2**, because it adsorbs more guest water (1.39%) due to its greater hydrophilicity.[42,55]

In compounds **1** and **2**, the proton conductivity is changed dynamically by humidity, by more than six and four orders of magnitude, respectively. This behavior is comparable to that of compound $\{(NH_4)_2(adp)[Zn_2(C_2O_4)_3]\cdot nH_2O\}_n$, whose negligible proton conductivity with a value of about 10^{-12} $(\Omega\cdot cm)^{-1}$ at RT increased to about 10^{-3} $(\Omega\cdot cm)^{-1}$ at 25 °C and 95% RH.[53,55] Also to that of $\{[(CH_3)_2NH_2]_2[Li_2Zr(C_2O_4)_4]\}_n$, which shows an abrupt increase in proton conductivity from $<10^{-9}$ to 3.9×10^{-5} $(\Omega\cdot cm)^{-1}$ at 17 °C (E_a = 0.64 eV) upon exposure to humidity of 67%.[59] These reported compounds exhibit very good guest-induced switchable proton conductivity and have the potential to be used as conductivity-switching devices in response to the external stimuli of atmospheric composition.[14]

Magnetization Study. The magnetization of compounds **1** and **2** is shown in Figures 4 and 5, respectively, with temperature dependence of magnetization $M(T)$, Curie-Weiss plot $\chi^{-1}(T)$ and field dependence of magnetization $M(H)$. The Curie-Weiss fit (left insets) of the high temperature part of $\chi^{-1}(T)$ gives the Curie constant C of (25.8±0.2) emu K mol^{-1} Oe^{-1} (**1**) and (25.7±0.2) emu K mol^{-1} Oe^{-1} (**2**), which are consistent with the paramagnetic state of the

magnetic manganese(II) and chromium(III) ions present in the compounds. These values are also evident in the temperature dependence of the χT product for **1** and **2** above 50 K (Figure S13). The values of the Weiss parameters θ after statistical analysis are (1±1) K (**1**) and (2.6±0.8) K (**2**). Due to their smallness and because of relatively large standard deviations coming from the application of the Curie-Weiss law only to high temperature region (above 50 K) where the sample signal is small and θ is sensitive to any minor inaccuracy in the subtraction of the background, the conclusions from the obtained Weiss parameters can not be discussed without doubts. Relatively small Weiss parameters could usually point to the negligible magnetic interactions, but taking into account the observed unusual shapes of the $M(T)$ and $M(H)$ curves, as well as $\chi T(T)$ dependence, the magnetic behavior is quite different from the paramagnetic one. Namely, the $M(T)$ curves of both compounds undoubtedly indicate the magnetic phase transition at 4.45 K, which is taken as a point of splitting between the zero-feld cooled and field-cooled magnetization curves. Another feature deserving attention is the broad maximum on the $M(T)$ curves that appears just slightly above the mentioned transition temperature. Considering the crystal structure of **1** and **2**, this maximum can appear as a signature of low-dimensional magnetism.

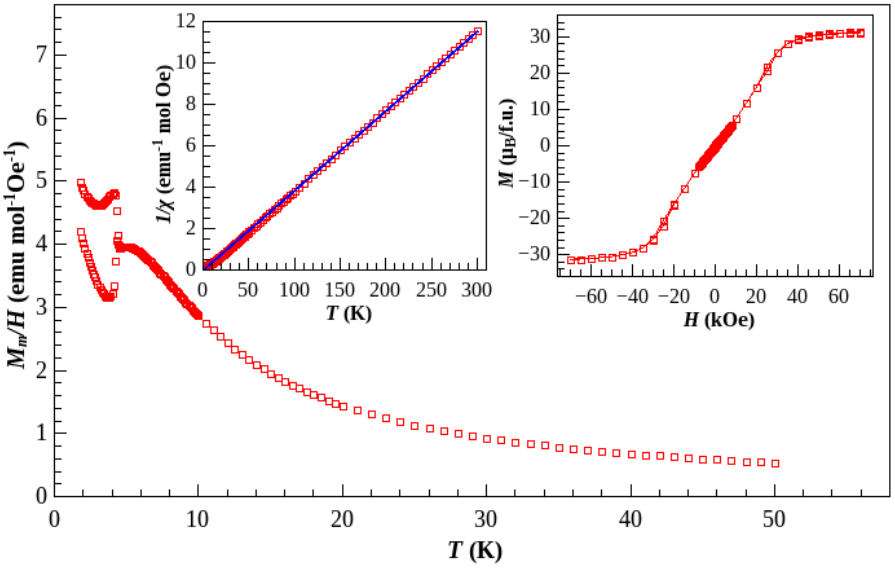

Figure 4. Temperature dependence of magnetization for $\{[NH(CH_3)_2(C_2H_5)]_8[Mn_4Cl_4Cr_4(C_2O_4)_{12}]\}_n$ (**1**) measured in 100 Oe. Left inset: Susceptibility measured in 1 kOe presented in the form of a Curie-Weiss plot with fitting line. Right inset: Field dependence of magnetization at temperature of 2 K.

First candidates for low-dimensional 1D magnetism are the zig-zag chains in the *a*-axis direction containing Mn^{2+} and Cr^{3+} ions bridged by bis(bidentate) oxalate group (Figure 1), which is known to transfer relatively large super-exchange interaction.[60] Second, these chains, whose magnetic interactions are the strongest and define these low-dimensional magnetic correlations, interact in the anionic layer with each other (Mn^{2+} and Cr^{3+} ions are bridged by monodentate-bidentate oxalate group; Figure 1) in the *c*-axis direction and form magnetic planes as 2D arrays of strongly correlated spins at temperatures slightly above the temperature of the long-range magnetic phase transition. Both 1D spin chains and 2D magnetic planes can produce maximum on $M(T)$ at temperatures above the long-range magnetic order, provided that there is an antiferromagnetic interaction, either along the chain in the 1D case or along one of the two in-

plane directions in 2D case. To exclude the unfavourable case in previous sentence, we examine the $M(H)$ curves which indicate that saturation magnetization of both **1** and **2** is approximately 32 Bohr magnetons per formula unit (4 Mn^{2+} and 4 Cr^{3+} ions), meaning that the spins are ferromagnetically oriented in larger magnetic fields, which is possible only for ferromagnetic super-exchange along the chains.

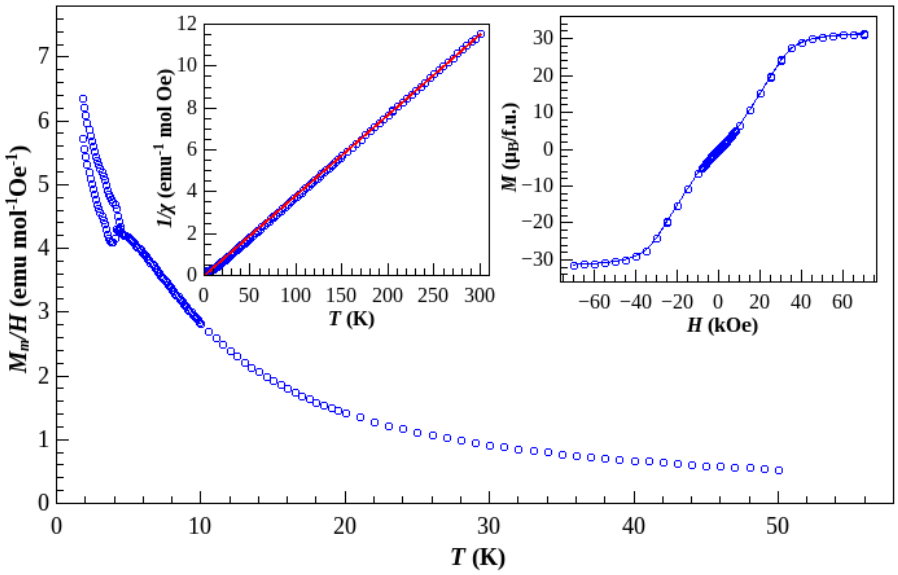

Figure 5. Temperature dependence of magnetization for $\{[NH(CH_3)(C_2H_5)_2]_8[Mn_4Cl_4Cr_4(C_2O_4)_{12}]\}_n$ (**2**) measured in 100 Oe. Left inset: Susceptibility measured in 1 kOe presented in the form of a Curie-Weiss plot with fitting line. Right inset: Field dependence of magnetization at temperature 2 K.

Namely, in the case of the antiferromagnetic ones, the state of the spin chain in this field should be ferrimagnetic, with much lower magnetization saturation. Therefore, the antiferromagnetic planes are formed from the ferromagnetic chains interacting antiferromagnetically over the bidentate-monodentate oxalate bridges. It is known from previous investigation[26,27,61] that such mode of bridging can provide a small antiferromagnetic interaction,

which is strong enough to correlate the spins within the planes below 5 K due to the large spins, as can be seen from the peaks in $M(T)$ (Figures 4 and 5). It is also worth mentioning that the modelling of the magnetization data above the transition temperature fails when the existence of the intrachain interaction (chains are considered in the finite ring approximation) and the local anisotropy of Cr and Mn (axial zero field splitting) are the only parameters taken into account. Unfortunately, it is practically impossible to include the interaction between the chains in the model, even with a mean-field approach, since the basic model is already very computationally intensive due to the high dimensionality of the Hilbert space.

Upon further cooling, the sudden change of magnetization is observed at 4.45 K, as shown in Figures 4 and 5 for a field of 100 Oe. The measurements made by the ZFC and FC methods differ significantly below this temperature, demonstrating the magnetic irreversibility typical of the long-range magnetically ordered systems.[26,31] At a higher field of 1000 Oe at the same temperature of 4.3–4.4 K, only a small bump is visible, which is common for such metal-organic systems[31] and measurement at smaller fields is necessary to observe the magnetic phase transition. This phase transition to long-range magnetic order is triggered by the third small interaction between the layers, possibly originate from a super-exchange interaction between the magnetic planes, which cannot be determined from the performed experiments and the used techniques. The $M(H)$ curves additionaly confirm the above considerations. Indeed, shape of the $M(H)$ points that the system is not pure 1D ferromagnet, but the slope at fields below the saturation suggests that there are some antiferromagnetic correlations that must be overcome at stronger fields. This is clearly evident as the inflection in $M(H)$ at roughly 20 kOe. Now it is more clear why the Weiss parameter does not give some realistic strength of the ferromagnetic interaction along the chains; Weiss parameter is relatively small because the antiferromagnetic

interactions along other two directions decrease the overall mean field. In such a case, the Weiss parameter is actually only a rough approximation, and its full justification applies only in magnetically isotropic and homogeneous system of high dimension (3D or 4D as ideal).

The magnetism of the quasi-two-dimensional structures of several $Mn^{II}Cr^{III}$ networks was studied previously, and the reported results were explained by a magnetic ordering characterized as soft ferromagnetism.[23,24,62–67] The transition temperatures ranged from 4 to 8 K are comparable to those observed in **1** and **2**. However, the reported structures have a 2D honeycomb arrangement, resulting in the saturated ferromagnetic moments within the planes and small interaction between the planes. Coordination polymers **1** and **2** exhibit a completely various structural topology, where the interconnections between the metal ions within the oxalate planes, together with a weak interaction between the planes, lead to the different dimensionality of the observable spin correlations with cooling, resulting finally in the phase transition at 4.45 K.

Ultimately, the question of the magnetic state in compounds **1** and **2** can not be completely and exactly answered, but the ground magnetic state can be described as follows: ferromagnetic alternate chains containing Mn^{2+} and Cr^{3+} ions bridged by a bis(bidentate) oxalate group interact mutually antiferromagnetically, resulting in strongly correlated antiferromagnetic planes that, under the influence of another weak interaction between the planes, lead to the long-range antiferromagnetic order. Although the interchain and interplane interactions are much smaller than the dominant intrachain super-exchange, the large spin of the metal centres enhances the interactions and makes the phase transition at 4.45 K visible. The existence of the magnetic transition is also supported by the AC magnetic susceptibility measurements [$\chi_{ac}(T)$ in Figure S13], where a clear peak appears at 4.45 K. Moreover, the broad maximum of $\chi_{ac}(T)$ centered at 5.2 K is in agreement with the discussed low-dimensional magnetism. The imaginary component

of AC susceptibility is near to zero in the measured temperature interval and without any features within the noise level.

Because of the small secondary magnetic interactions, it is actually possible to saturate the magnetization with fields of several Tesla, i.e. to move from the antiferromagnetic ground state to the ferromagnetic state at high fields. This would not be possible with strong intrachain antiferromagnetic interactions, which is additional argument in favor of above discussion. Finally, it should be noted that the $M(T)$ dependence around 4.45 K does not seem to be representative of a purely antiferromagnetic transition. It is more likely that a weak ferromagnetic ordering coming from canted antiferromagnetic sublattice is realised, originating from the anisotropic terms of the magnetic interactions whose existence is possible due to locally non-centrosymetric bridges in the structures of **1** and **2**. This and the above are very motivating for further magnetic study of this interesting system using other methods and techniques.

CONCLUSIONS

In summary, two novel [$Mn^{II}Cr^{III}$] coordination polymers exhibiting long-range antiferromagnetic ordering and very high proton conductivity have been rationally designed and successfully prepared. A crystallographic study of these isostructural compounds reveals a structure based on irregular 2D oxalate-bridged anionic layers $[Mn_4Cl_4Cr_4(C_2O_4)_{12}]_n^{8n-}$ interleaved by the hydrogen-bonded templating cations $(CH_3)_2(C_2H_5)NH^+$ (**1**) or $(CH_3)(C_2H_5)_2NH^+$ (**2**). The layer-cation interaction leads to a distance between the layers of ~8.5 Å, which is sufficient to accommodate several water molecules. The studied compounds **1** and **2** show proton conductivity that increases with RH to a much higher value of 1.60×10^{-3} $(\Omega \cdot cm)^{-1}$ at 90% RH and 9.6×10^{-4} $(\Omega \cdot cm)^{-1}$ at 94% RH, respectively**.** The proton conduction at ~10% RH is mediated by the hydrogen bonds of the bimetallic layer and alkyl-substituted ammonium

cations, whereas at ~80% RH additional five (**1**) and four (**2**) water molecules are responsible for the high proton conduction. The efficient proton conduction of **1** compared to **2** is explained by the relative hydrophilicity of the cationic ions. Because compounds **1** and **2** exhibit an increase in conductivity of six and four orders of magnitude, respectively, with increasing relative humidity, they indicate the potential switching behaviors triggered by water molecules. Magnetization at high temperature confirms the spin states of 5/2 for Mn^{2+} and 3/2 for Cr^{3+} ion, and cooling reveals the low-dimensional antiferromagnetic correlations evolving to long-range magnetic order. Considering the temperature and field dependence of the magnetization, the magnetic ground state can be described as ferromagnetic alternating spin chains [Mn^{2+} and Cr^{3+} ions bridged by a bis(bidentate) oxalate group] that generate antiferromagnetic planes by weak interaction with each other [Mn^{2+} and Cr^{3+} ions bridged by a bidentate-monodentate oxalate group], which are then long-range ordered by much weaker interlayer interactions in a soft antiferromagnetic lattice. This study confirms that the use of oxalate-bridged bimetallic complexes with hydrophilic cations appears promising for the producing multifunctional materials.

ASSOCIATED CONTENT

Supporting Information

The Supporting Information is available free of charge on the ACS Publications website at https://….:

Experimental and simulated PXRD patterns (Figures S1 and S2), selected distances and geometric parameters of hydrogen bonds (Tables S1 and S2), ORTEP-3 drawings (Fiures S3 and S4), TGA and DTA curves (Figure S5), PXRD patterns of samples obtained by heating (Figure S6), IR spectra (Figure S7), selected absorption bands in the IR spectra

(Table S3), Nyquist plots (Figure S8), time-dependent conductivity tests (Figure S9), PXRD patterns prior to and after the humidity treatment (Figures S10 and S11), proton conductivity of 2D and 3D oxalate-bridged coordination polymers (Table S4), TG curves after the samples was exposed to a humid condition (Figure S12), temperature dependence of the product χT (Figure S13).

Accession Codes

CCDC 2237907 and 2237908 contain the supplementary crystallographic data for this paper. These data can be obtained free of charge via www.ccdc.cam.ac.uk/data_request/cif, or by emailing data_request@ccdc.cam.ac.uk, or by contacting The Cambridge Crystallographic Data Centre, 12 Union Road, Cambridge CB2 1EZ, UK; fax: + 44 1223 336033.

Funding

This work has been funded and supported by the Croatian Science Foundation Project No. IP-2019-04-5742.

Notes

The authors declare no competing financial interest.

Acknowledgement

D. B. and D. P. acknowledge the support of project CeNIKS cofinanced by the Croatian Government and the European Union through the European Regional Development Fund – Competitiveness and Cohesion Operational Programme (Grant KK.01.1.1.02.0013).

AUTHOR INFORMATION

Corresponding Author

***Dr. Marijana Jurić**

Ruđer Bošković Institute

Bijenička cesta 54

10000 Zagreb, Croatia

Phone: +385 1 4561189. Fax: +385 1 4680098.
E-mail: Marijana.Juric@irb.hr. (M.J.)

REFERENCES

(1) Chakraborty, G.; Park, I.-H.; Medishetty, R.; Vittal, J. J. Two-Dimensional Metal-Organic Framework Materials: Synthesis, Structures, Properties and Applications. *Chem. Rev.* **2021**, *121*, 3751–3891.

(2) Chen, L.; Zhang, X.; Cheng, X.; Xie, Z.; Kuang, Q.; Zheng, L. The function of metal–organic frameworks in the application of MOF-based composites. *Nanoscale Adv.* **2020**, *2*, 2628–2647.

(3) Wang, Q. I.; Astruc, D. State of the art and prospects in metal-organic framework (MOF)-based and MOF-derived nanocatalysis. *Chem. Rev.* **2020**, *120*, 1438–1511.

(4) Coronado, E.; Mínguez Espallargas, G. Dynamic magnetic MOFs. *Chem. Soc. Rev.* **2013**, *42*, 1525–1539.

(5) Espallargas, G. M.; Coronado, E. Magnetic functionalities in MOFs: From the framework to the pore. *Chem. Soc. Rev.* **2018**, 47, 533–557.

(6) Groom, C. R.; Bruno, I. J.; Lightfoot, M. P.; Ward, S. C.The Cambridge Structural Database. *Acta Crystallogr*. **2016**, *B72*, 171–179.

(7) Hurd, J. A.; Vaidhyanathan, R.; Thangadurai, V.; Ratcliffe, C. I.; Moudrakovski, I. L.; Shimizu, G. K. H. Anhydrous proton conduction at 150 °C in a crystalline metal–organic framework. *Nature Chem.* **2009**, *1*, 705–710.

(8) Levenson, D. A.; Zhang, J.; Gelfand, B. S.; Kammampata,.S. P.; Thangadurai, V.; Shimizu, G. K. H. Particle size dependence of proton conduction in a cationic lanthanum phosphonate MOF. *Dalton Trans.* **2020**, *49*, 4022–4029.

(9) Levenson, D. A.; Zhang, J.; Szell, P. M. J.; Bryce, D. L.; Gelfand, B. S.; Huynh, R. P. S.; Fylstra, N. D.; Shimizu, G. K. H. Effects of Secondary Anions on Proton Conduction in a Flexible Cationic Phosphonate Metal–Organic Framework. *Chem. Mater.* **2020**, *32*, 679–687.

(10) Bao, S.-S.; Shimizu, G. K. H.; Zheng, L.-M. Proton conductive metal phosphonate frameworks, Proton conductive metal phosphonate frameworks. *Coord. Chem. Rev.* **2019**, 378, 577–594.

(11) Bureekaew, S.; Horike, S.; Higuchi, M.; Mizuno, M.; Kawamura, T.; Tanaka, D.; Yanai, N.; Kitagawa, S. One-dimensional imidazole aggregate in aluminium porous coordination polymers with high proton conductivity. *Nature Mater.* **2009**, *8*, 831–836.

(12) Wu, X.; Liu, Z.; Guo, H.; Hong, Y.-L.; Xu, B.; Zhang, K.; Nishiyama, Y.; Jiang, W.; Horike, S.; Kitagawa, S.; Zhang, G. Host–Guest Assembly of H-Bonding Networks in Covalent Organic Frameworks for Ultrafast and Anhydrous Proton Transfer. *ACS Appl. Mater. Interfaces* **2021**, *13*, 37172–37178.

(13) Wu, X.; Hong, Y.-l.; Xu, B.; Nishiyama, Y.; Jiang, W.; Zhu, J.; Zhang, G.; Kitagawa, S.; Horike, S. Perfluoroalkyl-Functionalized Covalent Organic Frameworks with Superhydrophobicity for Anhydrous Proton Conduction. *J. Am. Chem. Soc.* **2020**, *142*, 14357–14364.

(14) Xiang, F.; Chen, S.; Yuan, Z.; Li, L.; Fan, Z.; Yao, Z.; Liu, C.; Xiang, S.; Zhang, Z. Switched Proton Conduction in Metal-Organic Frameworks. *J. Am. Chem. Soc. Au* **2022**, *2,* 1043–1053.

(15) Lim, D.-W.; Kitagawa, H. Proton transport in metal–organic frameworks. *Chem. Rev.* **2020**, *120*, 8416–8467.

(16) Ye, Y.; Gong, L.; Xiang, S.; Zhang Z.; Chen, B. Metal–Organic Frameworks as a Versatile Platform for Proton Conductors. *Adv. Mater.* **2020**, *32*, 1907090.

(17) Su, J.; He, W.; Li, X.-M.; Sun, L.; Wang, H.-Y.; Lan, Y.-Q.; Ding, M.; Zuo, J.-L. High Electrical Conductivity in a 2D MOF with Intrinsic Superprotonic Conduction and Interfacial Pseudo-capacitance. *Matter* **2020**, *2*, 711–722.

(18) Xie, X.-X.; Yang, Y.-C.; Dou, B.-H.; Li, Z.-F.; Li, G. Proton conductive carboxylate-based metal-organic frameworks. *Coord. Chem. Rev.* **2020**, *404*, 213100.

(19) Lim, D-W.; Kitagaw, H. Rational strategies for proton-conductive metal–organic frameworks. *Chem. Soc. Rev.* **2021**, *50*, 6349–6368.

(20) Lim, D.-W.; Sadakiyo, M.; Kitagawa, H. Proton transfer in hydrogen-bonded degenerate systems of water and ammonia in metal–organic frameworks. *Chem. Sci.* **2019**, *10*, 16–33.

(21) Clemente-Leon, M.; Coronado, E.; Martí-Gastaldo, C.; Romero, F. M. Multifunctionality in hybrid magnetic materials based on bimetallic oxalate complexes. *Chem. Soc. Rev.* **2011**, *40*, 473–497.

(22) Gruselle, M.; Train, C.; Boubekeur, K.; Gredin, P.; Ovanesyan, N. Enantioselective self-assembly of chiral bimetallic oxalate-based networks. *Coord. Chem. Rev.* **2006**, *250*, 2491–2500.

(23) Tamaki, H.; Zhong, Z. J.; Matsumoto, N.; Kida, S.; Koikawa, M.; Achiwa, N.; Hashimoto, Y.;Ōkawa, H. Design of metal-complex magnets. Syntheses and magnetic properties of mixed-metal assemblies $\{NBu_4[MCr(ox)_3]\}_x$ (NBu_4^+ = tetra(n-butyl)ammonium ion; ox^{2-} = oxalate ion; M = Mn^{2+}, Fe^{2+}, Co^{2+}, Ni^{2+}, Cu^{2+}, Zn^{2+}). *J. Am. Chem. Soc.* **1992**, *114*, 6974–6979.

(24) Decurtins, S.; Schmalle, H. W.; Oswald, H. R.; Linden, A.; Ensling, J.; Gütlich, P.; Hauser, A. A polymeric two-dimensional mixed-metal network. crystal structure and magnetic properties of $\{[P(Ph)_4][MnCr(ox)_3]\}$. *Inorg. Chim. Acta* **1994**, *216*, 65–73.

(25) Kanižaj, L.; Androš Dubraja, L.; Torić, F.; Pajić, D.; Molčanov, K.; Wenger ,E.; Jurić, M. Dimensionality controlled by light exposure: 1D versus 3D oxalate-bridged [CuFe] coordination polymers based on an $[Fe(C_2O_4)_3]^{3-}$ metallotecton. *Inorg. Chem. Front.* **2019**, *6*, 3327–3335.

(26) Kanižaj, L.; Barišić, D.; Torić, F.; Pajić, D.; Molčanov, K.; Šantić, A.; Lončarić I.; Jurić, M. Structural, Electrical, and Magnetic Versatility of the Oxalate-Based [CuFe] Compounds Containing 2,2′:6′,2″-Terpyridine: Anion Directed Synthesis. *Inorg. Chem.* **2020**, *59*, 18078–18089

(27) Molčanov, L.; Šenjug, P.; Barišić, D.; Pajić, D.; Molčanov, K.; Jurić, M. Oxalate-based $[Cu^{II}Cr^{III}]$ coordination compounds affected by the tridentate ligand, simple anion, and reactant ratio: structural and magnetic features. *Dalton Trans.* **2022**, *51*, 16292–16306

(28) Kanižaj, L.; Šenjug, P.; Pajić, D.; Pavić, L.; Molčanov, K.; Jurić, M. Magnetic and Electrical Behaviors of the Homo- and Heterometallic 1D and 3D Coordination Polymers Based on the Partial Decomposition of the $[Cr(C_2O_4)_3]^{3-}$ Building Block. *Materials* **2020**, *13*, 5341.

(29) Kanižaj, L.; Molčanov, K.; Torić, F.; Pajić, D.; Lončarić, I.; Šantić, A.; Jurić, M. Ladder-like [CrCu] coordination polymers containing unique bridging modes of $[Cr(C_2O_4)_3]^{3-}$ and $Cr_2O_7^{2-}$. *Dalton Trans.* **2019**, *48*, 7891–7898.

(30) Habjanič, J.; Jurić, M.; Popović, J.; Molčanov, K.; Pajić, D. A 3D Oxalate-Based Network as a Precursor for the $CoMn_2O_4$ Spinel: Synthesis and Structural and Magnetic Studies. *Inorg. Chem.* **2014**, *53*, 9633–9643.

(31) Jurić, M.; Pajić, D.; Žilić, D.; Rakvin, B.; Molčanov, K.; Popović, J. Magnetic order in a novel 3D oxalate-based coordination polymer $\{[Cu(bpy)_3][Mn_2(C_2O_4)_3]\cdot H_2O\}_n$. *Dalton Trans.* **2015**, *44*, 20626-20635.

(32) Burazer, S.; Molčanov, K.; Šantić, A.; Klaser, T.; Wenger, E.; Pajić, D.; Jagličić, Z.; Popović, J.; Jurić, M. Humidity-Sensing Properties of an 1D Antiferromagnetic Oxalate-Bridged Coordination Polymer of Iron(III) and Its Temperature-Induced Structural Flexibility. *Materials* **2021**, *14*, 5543.

(33) Brauer, G. Handbuch der präparativen anorganischen Chemie. F. Enke: Stuttgart, Germany, 1981.

(34) Rigaku, O. D. P.R.O. CrysAlis, version: 1.171.39.46, Rigaku Oxford Diffraction Ltd, Yarnton, England, 2018.

(35) Sheldrick, G. M. *SHELXT* - Integrated space-group and crystal-structure determination. *Acta Crystallogr.* **2015**, *A71*, 3–8.

(36) Farrugia, L. J. WinGX and ORTEP for Windows: an update. *J. Appl. Crystallogr.* **2012**, *45*, 849–854.

(37) Spek, A. L. Single-crystal structure validation with the program. PLATON. *J. Appl. Crystallogr.* **2003**, *36*, 7–13.

(38) Macrae, C. F.; Sovago, I.; Cottrell, S. J.; Galek, P. T. A.; McCabe, P.; Pidcock, E.; Platings, M.; Shields, G. P.; Stevens, J. S.; Towler, M.; Wood, P. A. Mercury 4.0: from visualization to analysis, design and prediction. *J. Appl. Crystallogr.* **2020**, *53*, 226–235.

(39) Blatov, V. A. Voronoi–dirichlet polyhedra in crystal chemistry: theory and applications. *Crystallogr. Rev.* **2004**, *10*, 249–318.

(40) Pardo, E., Train, C.; Gontard, G.; Boubekeur, K.; Fabelo, O.; Liu, H.; Dkhil, B.; Lloret, F.; Nakagawa, K.; Tokoro, H.; Ohkoshi, S.-I.; Verdaguer, M. High Proton Conduction in a Chiral Ferromagnetic MetalOrganic Quartz-like Framework. *J. Am. Chem. Soc.* **2011**, 1*33*, 15328–15331.

(41) Maxim, C.; Ferlay, S.; Tokoro, H.; Ohkoshi, S.-I.; Train, C. Atypical stoichiometry for a 3D bimetallic oxalate-based long-range ordered magnet exhibiting high proton conductivity. *Chem. Commun.* **2014**, *50*, 5629–5632.

(42) Sadakiyo, M.; Ōkawa, H.; Shigematsu, A.; Ohba, M.; Yamada, T.; Kitagawa, H. Promotion of Low-Humidity Proton Conduction by Controlling Hydrophilicity in Layered Metal-Organic Frameworks. *J. Am. Chem. Soc*. **2012**, *134*, 5472–5475.

(43) Sadakiyo, M.; Yamada, T.; Kitagawa, H. Hydroxyl Group Recognition by Hydrogen-Bonding Donor and Acceptor Sites Embedded in a Layered Metal–Organic Framework. *J. Am. Chem. Soc.* **2011**, *133*, 11050–11053.

(44) Ōkawa, H.; Sadakiyo, M.; Yamada, T.; Maesato, M.; Ohba, M.; Kitagawa, H. Proton-Conductive Magnetic Metal–Organic Frameworks, $\{NR_3(CH_2COOH)\}[M_a^{II}M_b^{III}(ox)_3]$: Effect of Carboxyl Residue upon Proton Conduction. *J. Am. Chem. Soc.* **2013**, *135*, 2256–2262.

(45) Ōkawa, H.; Shigematsu, A.; Sadakiyo, M.; Miyagawa, T.; Yoneda, K.; Ohba, M.; Kitagawa, H. Oxalate-Bridged Bimetallic Complexes $\{NH(prol)_3\}[MCr(ox)_3]$ (M = Mn^{II}, Fe^{II}, Co^{II}; $NH(prol)_3^+$ = Tri(3-hydroxypropyl)ammonium) Exhibiting Coexistent Ferromagnetism and Proton Conduction. *J. Am. Chem. Soc.* **2009**, *131*, 13516–13522.

(46) Clemente-León, M.; Coronado, E.; Galán-Mascarós, J.-R.; Gómez-García, C. J.; Intercalation of decamethylferrocenium cations in bimetallic oxalate-bridged two-dimensional magnets. *Chem. Commun.* **1997**, 1727–1728.

(47) Coronado, E.; Galán-Mascarós, J.-R.; Gómez-García, C.-J.; Ensling, J.; Gütlich, P. Hybrid Molecular Magnets Obtained by Insertion of Decamethylmetallocenium Cations into Layered, Bimetallic Oxalate Complexes: $[Z^{III}Cp^*_2][M^{II}M^{III}(ox)_3]$ (Z^{III}=Co, Fe; M^{III}=Cr, Fe; M^{II}=Mn, Fe, Co, Cu, Zn; ox=oxalate; Cp*=pentamethylcyclopentadienyl). *Chem. Eur. J.* **2000**, *6*, 552–563.

(48) Bénard, S.; Yu, P.; Audière, J. P.; Rivière, E.; Clément, R.; Guilhem, J.; Tchertanov, L.; Nakatani, K. Structure and NLO Properties of Layered Bimetallic Oxalato-Bridged Ferromagnetic Networks Containing Stilbazolium-Shaped Chromophores. *J. Am.Chem. Soc.* **2000**, *122*, 9444–9454.

(49) Jirák, Z.; Vratislav, S.; Zajíček, J. Oxygen Parameters and Debye-Waller Factors in $Mn_xCr_{3-x}O_4$ Spinels. *Phys. Stat. Sol.* **1976**, *37*, K47-K51.

(50) Nakamoto, K. Infrared and Raman Spectra of Inorganic and Coordination Compounds, 6th ed., John Wiley, New York, 2009.

(51) Xu, H.-B.; Wang, Z.-M.; Liu, T.; Gao, S. Synthesis, Structure, and Magnetic Properties of $(A)[Fe^{III}(oxalate)Cl_2]$ (A = Alkyl Ammonium Cations) with Anionic 1D $[Fe^{III}(oxalate)Cl_2]^-$ Chains. *Inorg. Chem.* **2007**, *46*, 3089–3096.

(52) Silverstein, R. M.; Bassler, C. G.; Morrill, T. C. Spectrometric Identification of Organic Compounds, John Wiley & Sons, New York, 1974.

(53) Sadakiyo, M.; Yamada, T.; Kitagawa, H. Rational Designs for Highly Proton-Conductive Metal−Organic Frameworks. *J. Am. Chem. Soc.* **2009**, *131*, 9906–9907.

(54) Sadakiyo, M.; Yamada, T.; Kitagawa, H. Proton conductivity control by ion substitution in highly proton-conductive metal–organic framework. *J. Am. Chem. Soc.* **2014**, *136*, 13166–13169.

(55) Sadakiyo, M.; Yamada, T.; Honda, K.; Matsui, H.; Kitagawa, H. Control of Crystalline Proton-Conducting Pathways by Water- Induced Transformations of Hydrogen-Bonding Networks in a Metal−Organic Framework. *J. Am. Chem. Soc.* **2014**, *136*. 7701–7707.

(56) Sadakiyo, M.; Yamada, T.; Kitagawa, H. A study on proton conduction in a layered metal–organic framework, $Rb_2(adp)[Zn_2(ox)_3]\cdot 3H_2O$ (adp = adipic acid, ox^{2-} = oxalate). *Inorg. Chem. Commun.* **2016**, *72*, 138–140.

(57) Mon, M.; Vallejo, J.; Pasán, J.; Fabelo, O.; Train, C.; Verdaguer, M.; Ohkoshi, S.; Tokoro, H.; Nakagawa, K.; Pardo, E. A novel oxalate-based three-dimensional coordination polymer showing magnetic ordering and high proton conductivity. *Dalton Trans.* **2017**, *46*, 15130–15137.

(58) Nagarkar, S. S.; Unni, S. M.; Sharma, A.; Kurungot, S.; Ghosh, S. K. Two-in-one: inherent anhydrous and water-assisted high proton conduction in a 3D metal-organic framework. *Angew. Chem. Int. Ed.* **2014**, *53*, 2638–2642.

(59) Tominaka, S.; Coudert, F.; Dao, T. D.; Nagao, T.; Cheetham, A. K. Insulator-to-Proton-Conductor Transition in a Dense Metal–Organic Framework. *J. Am. Chem. Soc.* **2015***, 137* 6428–6431.

(60) Kahn, O. *Molecular Magnetism*. Wiley-VCH: New York, 1993.

(61) Vallejo, J.; Castro, I.; del Déniz, M.; Ruiz-Pérez, C.; Lloreta, F.; Julve, M.; Ruiz-García, R.; Cano, J. Magnetic coupling and spin topology in linear oxalato-bridged tetranuclear chromium(III)–copper(II) complexes with aromatic diimine ligands. *Polyhedron* **2013**, *52*, 1246–1255.

(62) Clemente-Leon, M.; Coronado, E.; López-Jordà, M. 2D and 3D bimetallic oxalate-based ferromagnets prepared by insertion of different Fe^{III} spin crossover complexes. *Dalton Trans.* **2010**, *39*, 4903–4910.

(63) Clemente-León, M.; Coronado, E.; Dias, J. C.; Soriano-Portillo, A.; Willett; R. D. Synthesis, Structure, and Magnetic Properties of [(*S*)-

[PhCH(CH_3)N(CH3)$_3$]][Mn(CH_3CN)$_{2/3}$Cr(ox)$_3$]·(CH_3CN)_(solvate), a 2D Chiral Magnet Containing a Quaternary Ammonium Chiral Cation. *Inorg. Chem.* **2008**, *47*, 6458–6463.

(64) Clemente-León, M.; Coronado, E.; López-Jordà, M. 2D Bimetallic Oxalate-Based Ferromagnets with Inserted [Fe(4-Br-sal$_2$-trien)]+ and [Fe(3-R-sal$_2$-trien)]+ (R = Br, Cl and CH_3O) Fe^{III} Spin-Crossover Complexes. *Eur. J. Inorg. Chem.* **2013**, 753–762.

(65) Maxim, C.; Ferlay, S.; Train, C. Dialkyl-substituted monoamidinium-templated oxalate-based noncentrosymmetric 2D compounds. *C. R. Chimie* **2019**, *22*, 534–540.

(66) Coronado, E.; Galán-Mascarós, J. R.; Martí-Gastaldo, C.; Waerenborgh, J. C.; Gaczyński, P. Oxalate-Based Soluble 2D Magnets: The Series [K(18-crown-6)]$_3$[M^{II}_3(H_2O)$_4${M^{III}(ox)$_3$}$_3$] (M^{III} = Cr, Fe; M^{II} = Mn, Fe, Ni, Co, Cu; ox = $C_2O_4^{2-}$; 18-crown-6 = $C_{12}H_{24}O_6$). *Inorg. Chem.* **2008**, *47*, 6829–6839.

(67) Coronado, E.; Galán-Mascarós, J. R.; Martí-Gastaldo, C. Synthesis and Characterization of a Soluble Bimetallic Oxalate-Based Bidimensional Magnet: [K(18-crown-6)]$_3$[Mn$_3$(H_2O)$_4${Cr(ox)$_3$}$_3$]. *Inorg. Chem.* **2006**, *45*, 1882–1884.

TABLE OF CONTENTS SYNOPSIS

Two coordination polymers $\{[A]_8[Mn_4Cl_4Cr_4(C_2O_4)_{12}]\}_n$ [A = $(CH_3)_2(C_2H_5)NH^+$ (**1**) and $(CH_3)(C_2H_5)_2NH^+$ (**2**)] show remarkable structural, electrical and magnetic features: atypical 2D oxalate-bridged anionic layers with $4{\cdot}8^2$ topology, humidity sensing properties, high proton conductivity, and long-range antiferromagnetic order.